




Effects of shear test temperatures and conditions on mechanical properties of Sn–Ag flip-chip solder bumps

Min-Haeng Heo¹, Dong-Hwan Lee¹, Min-Seong Jeong¹, and Jeong-Won Yoon^{1,*} 

¹Department of Advanced Materials Engineering, Chungbuk National University, 1 Chungdae-ro, Seowon-gu, Cheongju 28644, Chungbuk, Korea

Received: 4 February 2022

Accepted: 25 February 2022

Published online:
9 March 2022

© The Author(s), under exclusive licence to Springer Science+Business Media, LLC, part of Springer Nature 2022

ABSTRACT

Lately, as electronic devices are continually becoming smaller, thinner, and multifunctional, there has been a growing demand for highly integrated packaging technologies. Accordingly, the application of flip-chip bonding technology has significantly increased to meet these demands. Therefore, the reliability evaluation of the micro-sized solder bumps used in flip-chip bonding and an understanding of the relevant mechanical properties has become essential. To evaluate the properties and reliability of Sn–2.3Ag (in wt%) flip-chip bump in various environments, this study compared the results of shear tests performed under three varying conditions, viz., shear heights (10, 15, 20, and 25 μm), shear rates (50, 100, 150, 200, 300, and 500 $\mu\text{m/s}$), and shear temperatures (25, 50, 100, 125, and 150 $^{\circ}\text{C}$). A global bond tester was used for the shear tests and scanning electron microscopy was used to observe and analyze the fracture surfaces and joint cross sections subsequent to the tests. The experimental analysis showed that the shear test conditions had a significant impact on the shear strength and joint mechanical properties of the flip-chip bumps. The shear strength tends to decrease as the shear height and temperature increase, whereas it tends to increase in correspondence with increase in the shear rate. The correlations between the results of the mechanical characterization according to these test conditions were comparatively analyzed.

1 Introduction

Rapid growth of the IT industry and the increasing demand for semiconductors in fields such as the Internet of Things (IoT), big data, cloud computing,

artificial intelligence, and application processors have led to the rapid development and miniaturization of semiconductor devices. In response, various advanced semiconductor packaging technologies have been developed to fabricate lighter, thinner, and

Address correspondence to E-mail: jwyoona@chungbuk.ac.kr

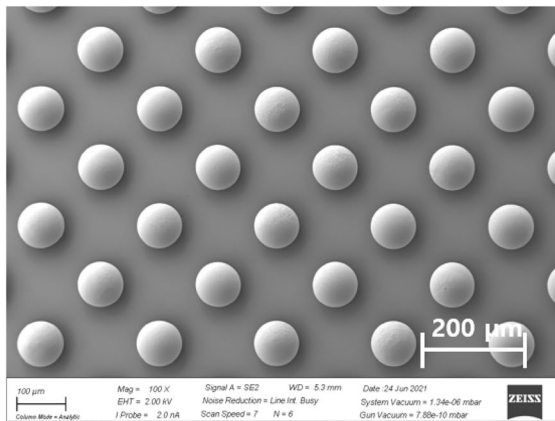
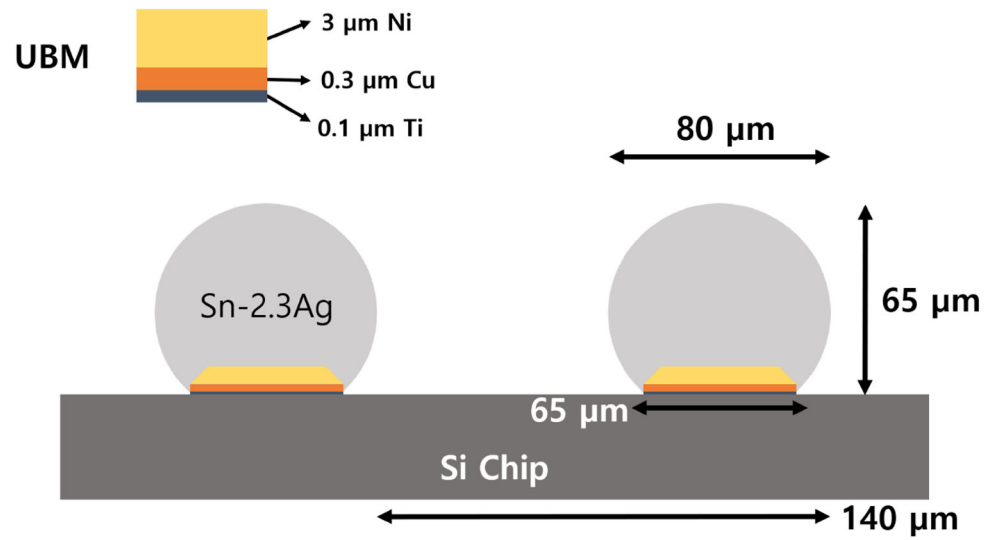
smaller semiconductors [1]. Among these, flip-chip bonding technology is one that is gaining significance and used widely in advanced semiconductor packaging technologies, such as package-on-package (PoP) and system-in-package (SiP) [2, 3]. Currently, two methods are commonly used for the electrical connections between semiconductor chip electrodes and external circuit electrodes: wire bonding and flip-chip bonding. The flip-chip bonding technology involves flipping a semiconductor chip and connecting it to a substrate or another chip using micro solder bumps on a two-dimensional array chip. The advantages of this method over wire bonding include a higher number of inputs and outputs (I/Os), which saves considerable space and reduces inductance owing to the short connection length, enabling the chip to meet the high-capacity, high-speed signal transmission requirements of technologically advanced products [4–7]. The semiconductor chips used in advanced products are becoming increasingly integrated; hence, the flip-chip bonding technique and solder bump used in this method need to be extremely reliable, because they have a significant impact on the overall reliability of the device. Currently, Sn–Ag binary solder bumps that are formed in batches on wafers via electrolytic plating methods are used as flip-chip bump materials, and studies are being undertaken to reduce the Ag content to reduce costs [8].

When used in advanced products that require higher reliability for aforementioned applications, the flip-chip joints are continuously subjected to various external mechanical and thermal stresses. Hence, their thermomechanical reliability needs to be evaluated, and a good understanding of the mechanical properties of micro sized solder bumps used for flip-chip bonding is also necessary. Although many studies on the mechanical properties of ball-grid-array-type solder joints and bulk-type tensile test joints have been performed, studies on micro sized Sn–Ag flip-chip solder bumps are still insufficient. In this study, three variables, namely, shear height, shear rate, and shear temperature, have been used in experiments to evaluate the properties of Sn–Ag flip-chip solder bumps under various environmental conditions. The mechanical properties of the Sn–Ag solder bump were evaluated via shear tests, and the joint reliability was assessed and compared via microstructural analysis of the fracture surfaces.

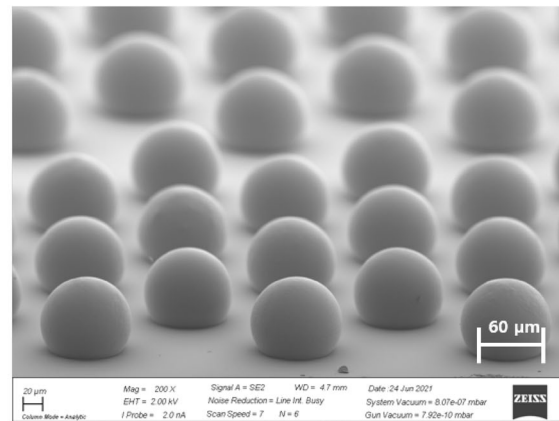
2 Experimental methods

The Sn-2.3Ag (wt%) solder bump was used for the shear test. The diameters of the solder bump and pad were 80 and 65 μm , respectively, while that of the bump pitch was 140 μm . The under-bump metallization (UBM) layer consisted of Ni, Cu, and Ti layers with thicknesses of 3, 0.3, and 0.1 μm , respectively. Figure 1 is a cross-sectional diagram of a solder bump depicting the thickness and structure of the UBM layer. The specimen was mounted with epoxy material for cross-sectional observation, polished, and etched for metallurgical cross-sectional observation. Figure 2 shows the scanning electron microscopy (SEM) and energy-dispersive X-ray spectroscopy (EDS) mapping images of the bump array and its cross-section. Shear tests were conducted under various test conditions using shear test equipment (DAGE 4000, Nordson DAGE, UK) to evaluate the mechanical properties of the flip-chip bump. Shear tests were conducted by varying the shear height, shear rate, and shear temperature to observe changes in the shear test characteristics of the flip-chip bump. The size of the shear tool used in the shear tests was 100 μm , which was specifically fabricated considering the size of the flip-chip bump to be evaluated. The shear strength, shear distance, and force–displacement (F – x) curves were measured. The detailed conditions for each shear test are presented in Tables 1, 2, and 3. Shear strength was calculated by dividing the measured shear force by the area of the pad. Figure 3 shows schematics of the shear tests conducted in this study. The shear tests under varying temperatures presented in Fig. 3b was performed by placing the bump-formed chip on a heating plate based on the temperature variation of the heating plate whose temperature was measured using a thermocouple. Subsequent to the shear test, the fracture surfaces of each joint were analyzed using SEM. Overall, thirty bumps were tested under each shear test condition, and the average values have been calculated and reported herein. Furthermore, the correlations between these experimental variables and the mechanical property evaluation results have been analyzed and discussed in this paper.

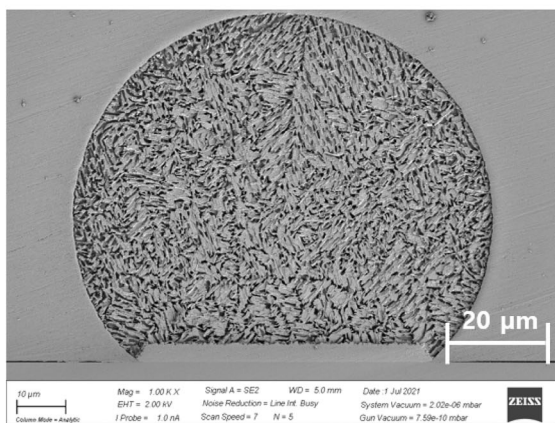
Fig. 1 Schematics of flip-chip bump and UBM structure



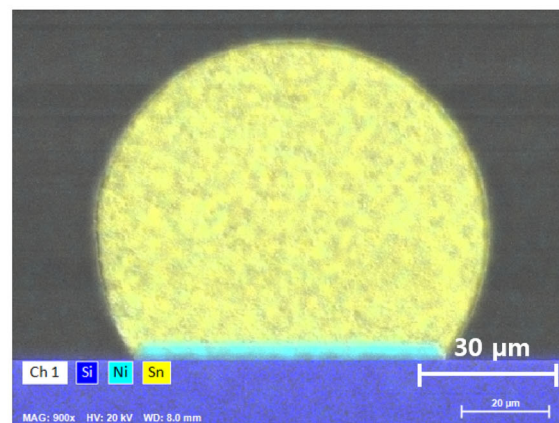
(a)



(b)



(c)



(d)

Fig. 2 SEM images of flip-chip bumps: **a** top view, **b** tilted view, **c** cross-section, and **d** EDS mapping image

Table 1 Bump shear test conditions under various shear heights

Speed (μm/s)	Height (μm)			
100	10	15	20	25
	(15.4%)	(23.1%)	(30.8%)	(38.5%)

(*%)—ratio of shear height to bump height

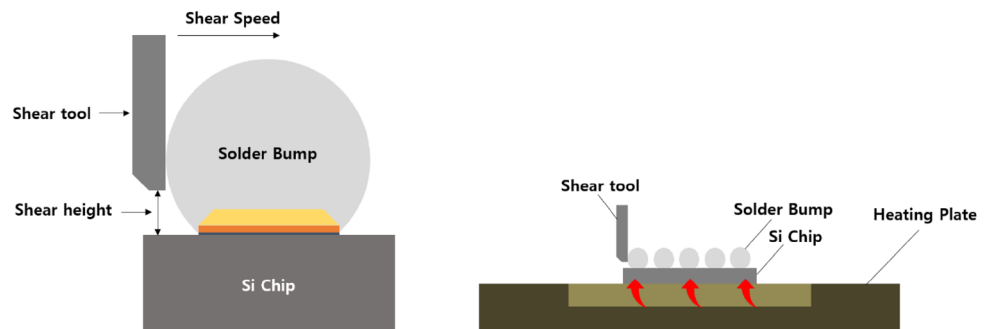
Table 2 Bump shear test conditions under various shear speeds

Height (μm)	Speed (μm/s)					
10	50	100	150	200	300	500

Table 3 Bump shear test conditions under various shear temperatures

Speed (μm/s)	Height (μm)	Temperature (°C)				
100	10	25	50	100	125	150

Fig. 3 Schematics of **a** bump shear test and **b** heating shear test



3 Results and discussion

3.1 Effect of shear height

After the bumping and reflow processes, Ni₃Sn₄ intermetallic phases formed at the interface between the Sn–Ag solder bump and the Ni UBM. The mechanical properties of the flip-chip bump were evaluated according to the shear height by conducting shear tests for each of the following four shear heights: 10, 15, 20, and 25 μm. These shear heights represent a shear height to bump height ratio of 15.4, 23.1, 30.8, and 38.5%, respectively (Table 1). Figure 4 presents the variation of the shear strength of a solder bump in relation to the shear height wherein the decreasing tendency of the shear strength in correspondence with increase in shear height can be

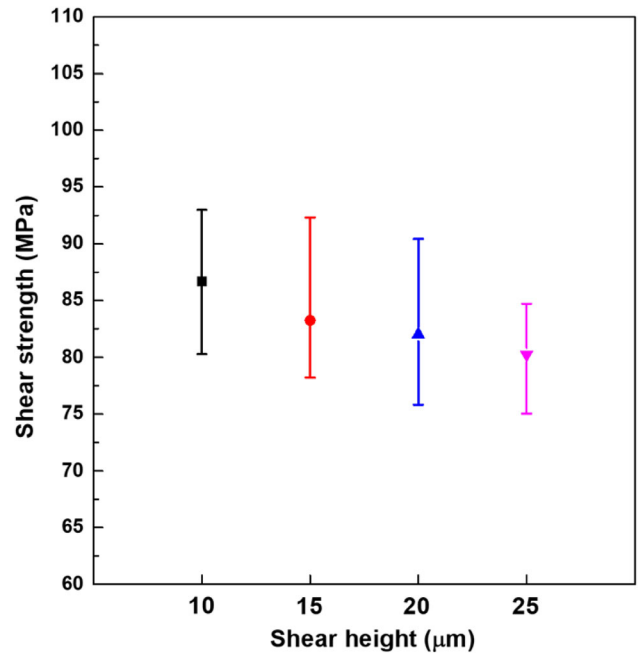


Fig. 4 Variations of shear strength with shear height

observed. The shear strength tends to decrease as the height of the shear test moves away from the joint interface. Kim et al. reported that the cause of the decrease in shear strength was the decrease in the initial contact area between the shear tool and bulk solder ball (or bump) as the shear height increased, which decreased the resistance of the solder bump to plastic deformation [9]. This trend can be interpreted using the following equation:

$$F/A \propto x/H \text{ (shear strength vs shear strain)}$$

where, *F* represents the shear force, *A* the shear area, *x* the shear distance, and *H* the shear height [10]. Figure 5 shows the variation in shear distance with variation in shear height, and it can be observed that corresponding with an increase in the shear height, the shear distance tends to increase. This is can be

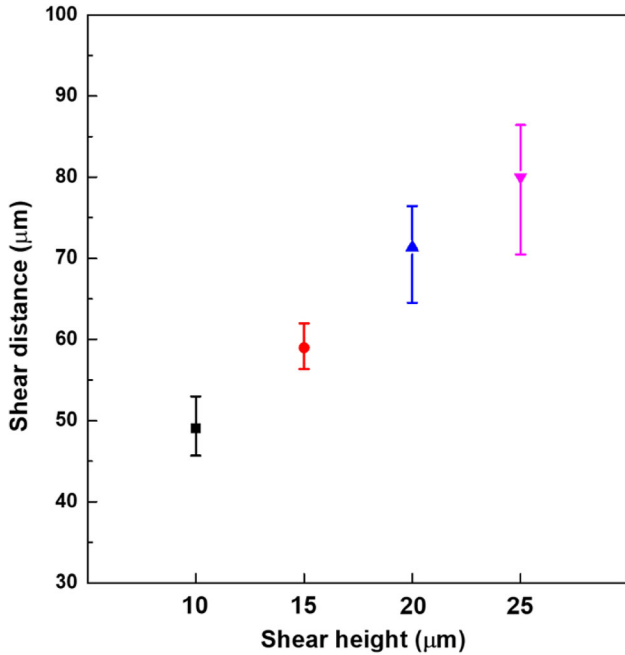


Fig. 5 Variations of shear distance with shear height

attributed to the fact that the area of the solder bump that was sheared increased during the actual shear test as the shear height increased. Figure 6 shows a representative force–displacement ($F-x$) curve for each shear height condition. It is worth noting that as the shear height increased, the maximum shear force

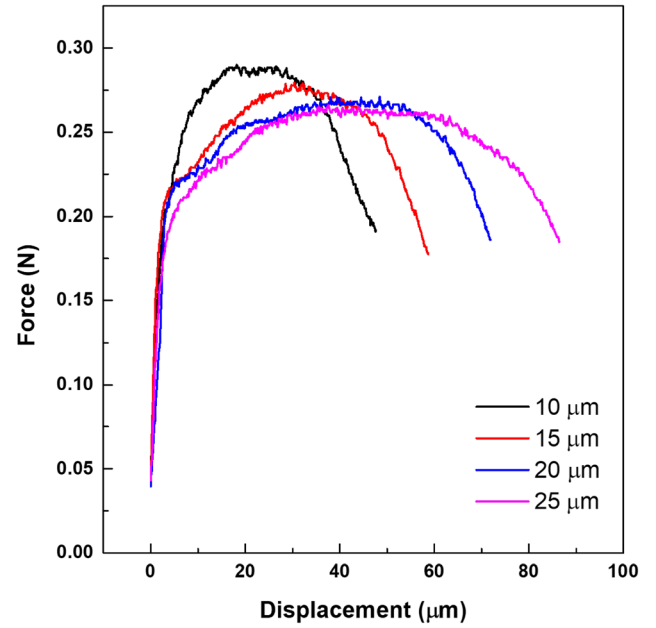
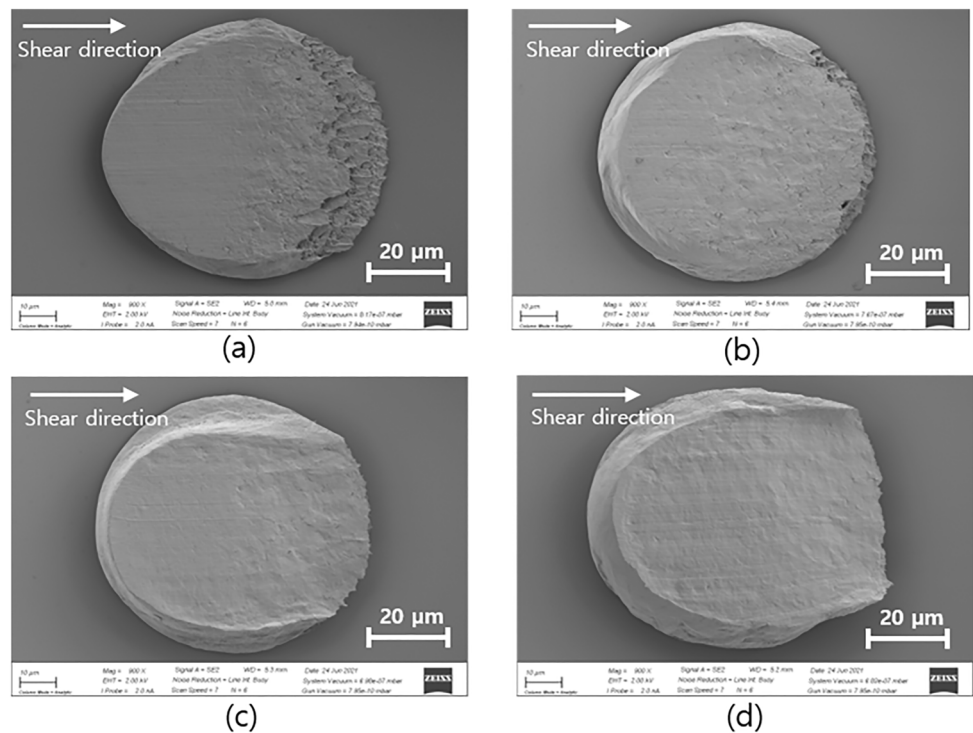


Fig. 6 Force–displacement ($F-x$) curve at various shear heights

decreased, and correspondingly the displacement increased. After the shear test, the fracture surface was subjected to SEM observation to determine the cause of the change in strength with respect to shear height. Figure 7 shows the representative SEM images of the fractured surfaces observed after the shear test for each condition. Based on the observation, it

Fig. 7 SEM images of fracture surfaces of solder bumps at different shear heights: **a** 10 μm, **b** 15 μm, **c** 20 μm, and **d** 25 μm



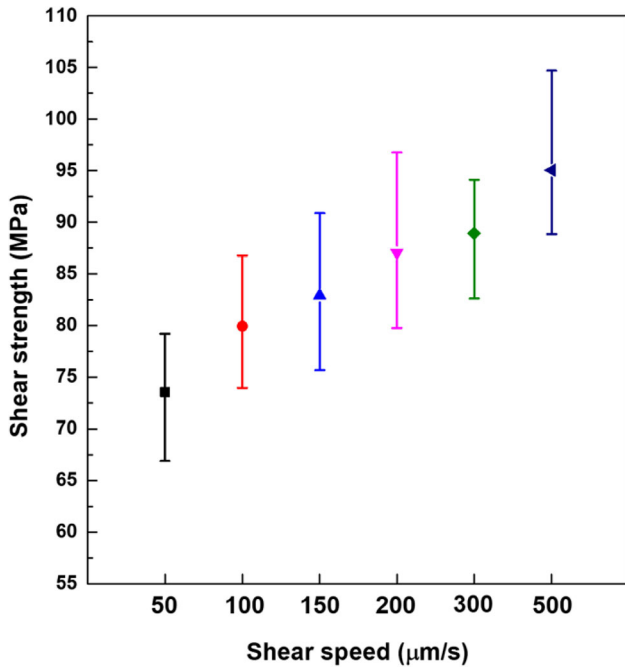


Fig. 8 Variations of shear strength with shear speed

can be concluded that all four shear height conditions resulted in ductile fractures within the solder bump. Further, it is evident that the rate of dimples on the fractured surface decreased, whereas the shear area increased in correspondence with increase in shear height. More specifically, under the shear height conditions of 20 and 25 μm, which represent 25% of the solder bump height or more, no dimples were observed and the solder was confirmed to have been stretched in the shear direction.

3.2 Effect of shear rate

The mechanical properties of the flip-chip bump were evaluated at different shear rates by fixing the shear height at 10 μm and shear tests were performed at six different shear rates, viz., 50, 100, 150, 200, 300, and 500 μm/s, and the results are presented in Figs. 8–10. Figure 8 shows the variation in shear strength in correspondence with shear rate, and it can be observed that the shear strength of the solder bump tends to increase with increasing shear rate. This can be interpreted as an increase in the strain rate with an increase in shear rate. Because the solder has a positive sensitivity to the strain rate, the dislocation movement increases proportionally to the strain rate. This results in an increase in the flow stress, which in turn increased the shear strength [11].

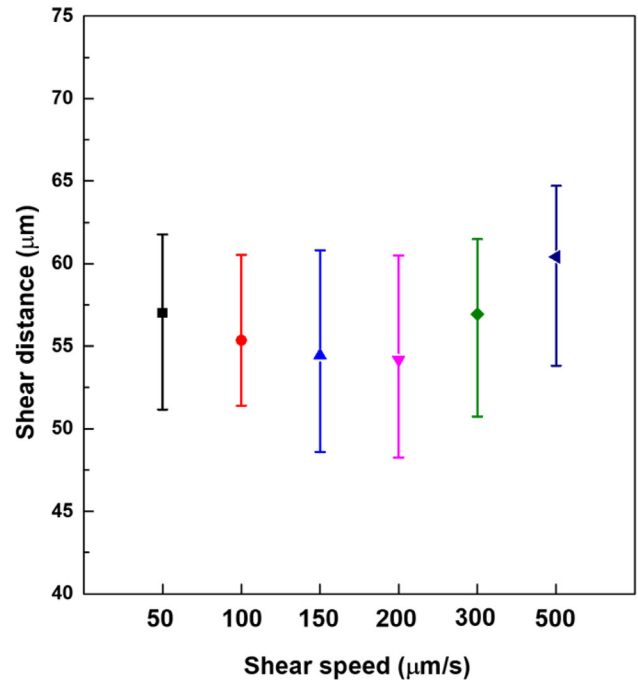


Fig. 9 Variations of shear distance with shear speed

Kim et al. reported that a Sn–37Pb solder bump showed an increasing tendency of shear force with increasing shear rate [12]. Additionally, Shohji et al. reported that Sn–3.0Ag–0.5Cu solder showed an increasing tendency of shear strength with an increase in the shear rate [13]. Shohji et al. also

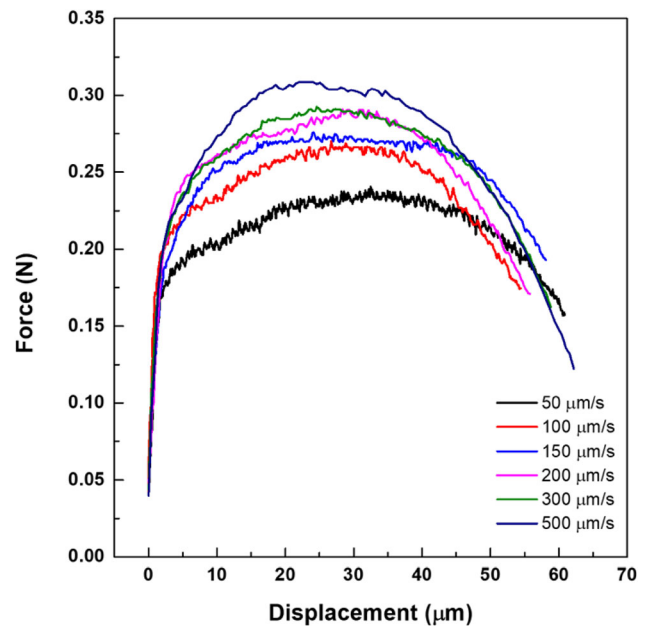


Fig. 10 Force–displacement ($F-x$) curve at various shear speeds

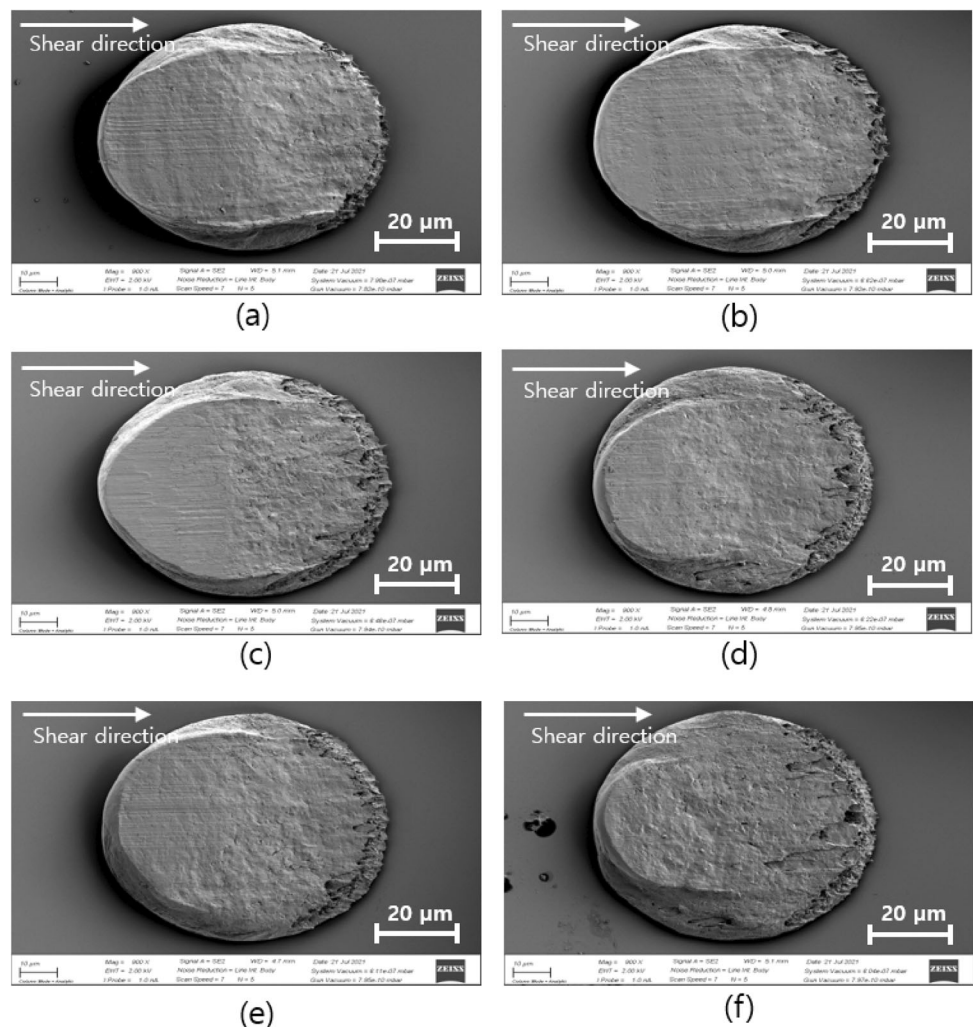
reported that, based on tensile tests, Sn–3.5Ag and Sn–3.5Ag–0.75Cu solders showed an increasing tendency of tensile strength with increasing strain rate [14]. Figure 9 shows the variation in the shear distance measurements corresponding to changes in the shear rate, and it is evident that the shear distance tends to decrease slightly corresponding to an increase in the shear rate between 50 and 200 $\mu\text{m/s}$, while on the contrary it has a tendency to increase slightly at shear rates of 300 and 500 $\mu\text{m/s}$. Regardless of the tendency to increase or decrease, the difference in the average shear distance between the shear rate conditions was minimal, thereby suggesting that the effect of the shear rate is not significant. Figure 10 shows the representative F – x curves for each shear rate condition and it can be observed that the shear force increased with the shear rate. Moreover, although there were minor differences between

the conditions, no significant change in displacement could be observed corresponding with change in the shear rate. After the shear test, the fracture surface was examined to determine the cause of the change in strength under varying shear rates, and the representative SEM images of the fracture surfaces for each condition are presented in Fig. 11. The observation of the fracture surface revealed ductile fracture in the solder bump under all shear rate conditions, and no significant difference was observed in the rate of dimpled fracture surface or fracture morphology in relation to the shear rate condition.

3.3 Effect of shear temperature

The mechanical properties of the flip-chip bump were evaluated according to the shear test temperature by performing shear tests at five different

Fig. 11 SEM images of fracture surfaces of solder bumps at different shear speeds: **a** 50 $\mu\text{m/s}$, **b** 100 $\mu\text{m/s}$, **c** 150 $\mu\text{m/s}$, **d** 200 $\mu\text{m/s}$, **e** 300 $\mu\text{m/s}$, and **f** 500 $\mu\text{m/s}$



temperatures, viz., 25, 50, 100, 125, and 150 °C. Table 4 lists the temperature settings of the shear tests, the actual temperatures measured with the thermocouple, and the calculated homologous temperature (T_H). The homologous temperature is defined as the ratio of the operating temperature to the melting temperature of the solder material, based on the absolute temperature scale (K). The melting temperature of Sn-2.3Ag was assumed to be 221 °C for the purpose of calculations [15]. Figure 12 shows the variation in the shear strength in correspondence with the shear test temperature, and it is evident that the shear strength of the solder bump tends to decrease with increasing shear test temperature. For example, the shear strengths measured at 25 and

150 °C were 82 and 43 MPa, respectively, thereby indicating that the measured shear strength of the Sn–Ag flip-chip bump decreased by approximately 48% as the temperature increased from 25 to 150 °C. Table 5 summarizes the percentage reduction in shear strength in comparison with that at 25 °C. It is believed that the change was caused by softening of the solder alloy owing to the heat applied from the heating plate. According to the phase diagram of the Sn–Ag system, the eutectic phases of β -Sn and Ag_3Sn are stable in the temperature range from room temperature to the eutectic temperature of 221 °C. Therefore, the phase change of the eutectic microstructure did not occur in the temperature range from 25 to 150 °C at which tests were

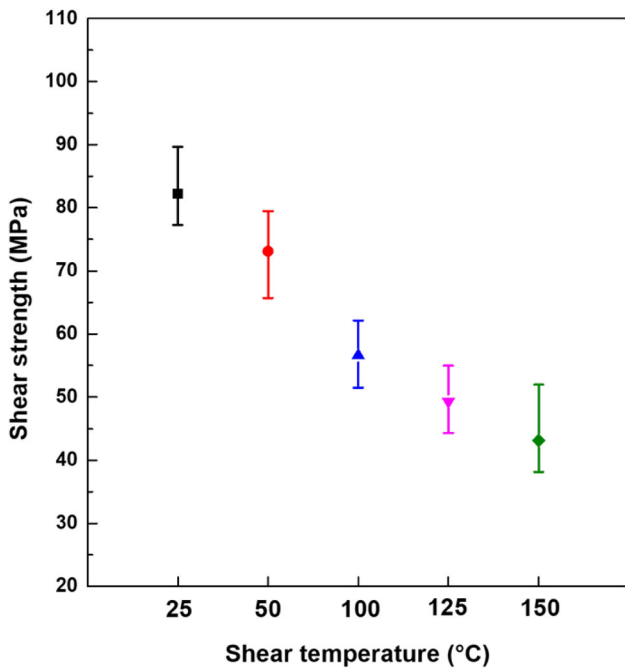


Fig. 12 Variations of shear strength with shear temperature

Table 4 Setting temperatures, actual measured temperatures, and homologous temperatures (T_H) in the shear test

Setting temperature (°C)	Measured temperature (°C)	T_H
25	30.1	0.61
50	46.9	0.65
100	85.8	0.73
125	107.2	0.77
150	138.3	0.83

T_H Homologous temperature

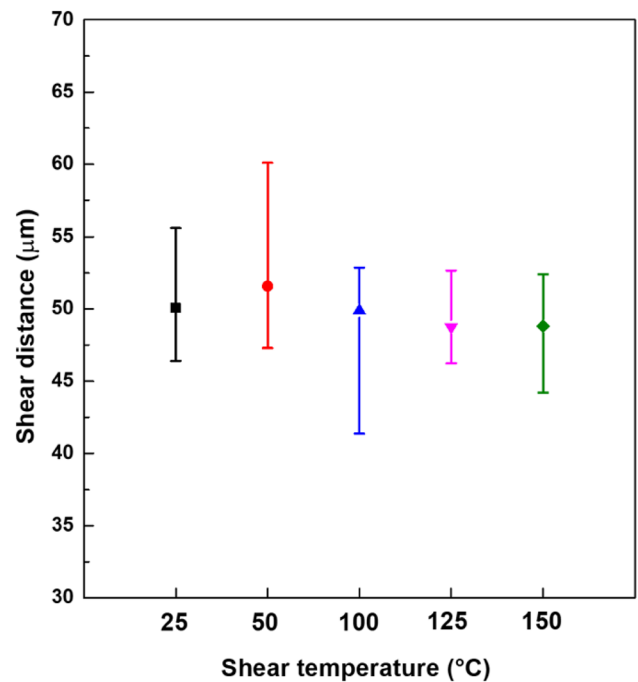


Fig. 13 Variations of shear distance with shear temperature

Table 5 Rate of shear strength decrease compared with that at 25 °C

Temperature (°C)	Shear strength reduction rate (%)
50	11
100	31
125	40
150	48

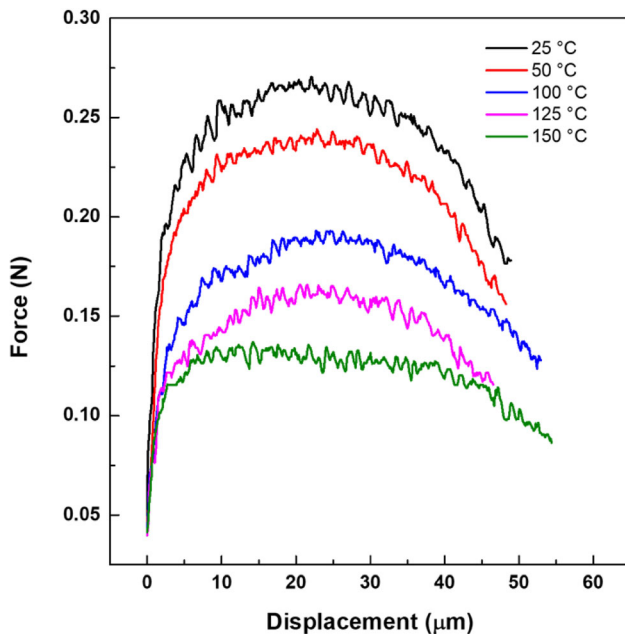


Fig. 14 Force–displacement (F – x) curve at various shear temperatures

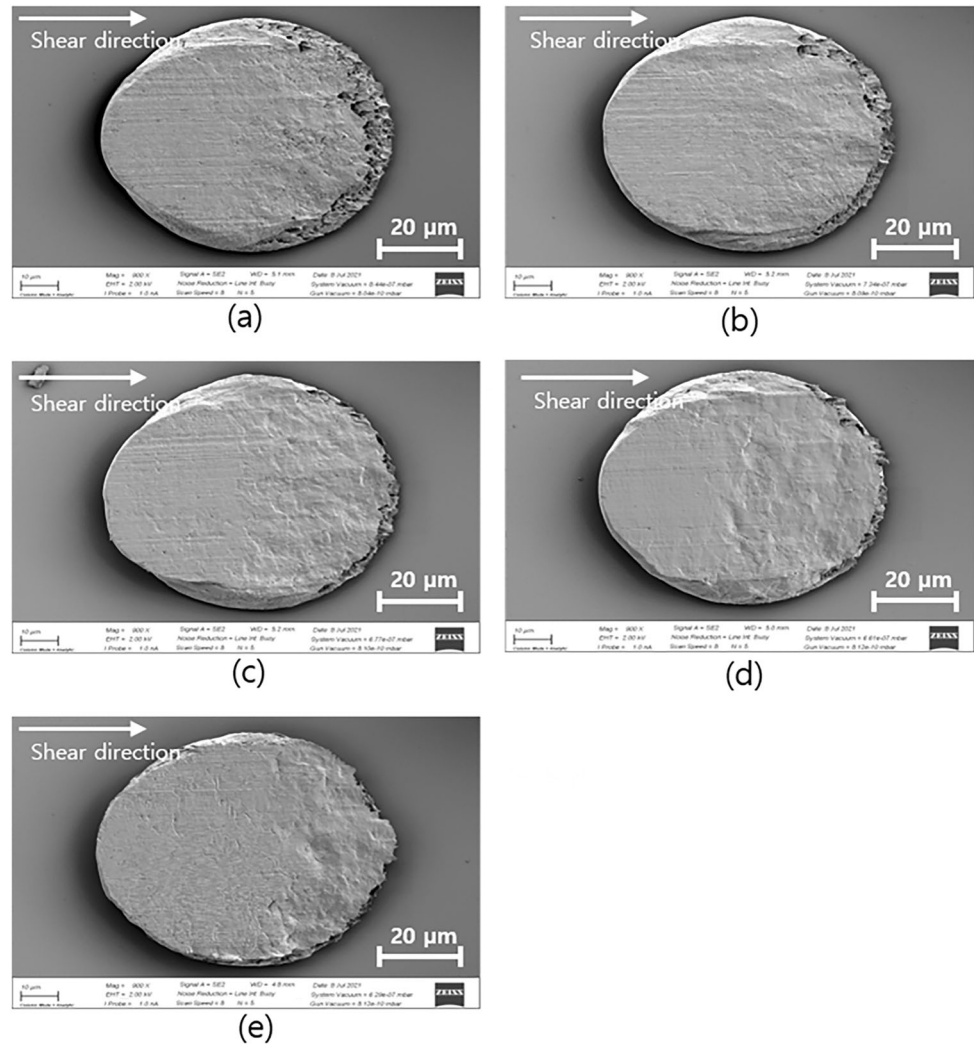
conducted in this study. Mohammadi et al. reported that the solder with the composition Sn–0.7Cu– x SiC showed a decrease in shear strength with an increase in shear temperature. Although the solder alloy composition in the aforementioned reference was different from that used in this experiment, a similar tendency was observed for the Sn-dominant solder alloy as well [16]. Huang et al. reported that tensile tests performed in the temperature range from -40 to 120 °C revealed relatively high tensile strengths at low temperatures and low tensile strengths at high temperatures [17]. Figure 13 shows the variation in the shear distance with variation in the shear temperature, and it can be observed that the averages of shear distance corresponding to shear temperature were not significantly different, thereby suggesting that the effect of temperature on shear distance was not significant. Figure 14 shows a representative F – x curve for each shear test temperature condition, and the curves indicate that the maximum shear force decreased with increasing shear test temperature; it is worth noting, however, that the change in displacement with increase in temperature is not significant. After the shear test, the fracture surface was

examined to determine the cause of the strength changes corresponding with changes in shear temperature. Figure 15 shows the representative SEM images of the fracture surface under each condition. The observations revealed that ductile fracture occurred in the solder bumps under all five test temperature conditions, and the rate of dimpled fracture surface decreased with increasing shear test temperature.

4 Conclusion

Shear tests were conducted with three variables, namely shear height, shear rate, and shear temperature, to determine the mechanical reliability of the Sn–2.3Ag flip-chip solder bumps in various environments. In the case of shear tests with variable shear heights, tests were conducted at heights of 10, 15, 20, and 25 μm . The results showed that shear strength decreased with increasing shear height, whereas the shear displacement tended to increase with increasing shear height. Further, analysis of the fracture surfaces after the shear test showed that the rate of dimpled fracture surfaces decreased with increasing shear height. In the case of the shear tests under varying shear rates, the shear strength increased as the shear rate increased. There was no significant change in the shear distance or displacement with variations in the shear rate. Following the shear test, fracture surface analysis demonstrated no significant differences in the fracture surface morphology corresponding with variations in shear rate: ductile fracture behavior was observed under all conditions. In the case of shear tests under varying shear temperatures (i.e., 25, 50, 100, 125, and 150 °C), the shear strength tended to decrease as the temperature increased. As the shear test temperature increased from 25 to 150 °C, the measured shear strength of the Sn–Ag flip-chip bump decreased by approximately 48%. A fracture surface analysis conducted after the shear test revealed that ductile fracture was observed under all the temperature conditions, and the rate of dimpled fracture surfaces decreased with an increase in the shear test temperature.

Fig. 15 SEM images of fracture surfaces of solder bumps at different shear temperatures: **a** 25 °C, **b** 50 °C, **c** 100 °C, **d** 125 °C, and **e** 150 °C



Acknowledgments

This work was supported by the National Research Foundation of Korea(NRF) grant funded by the Korea government(MSIT) (No. 2021R1A2C1009714) and Korea Institute for Advancement of Technology(KIAT) grant funded by the Korea Government (MOTIE)(P0008458, HRD Program for Industrial Innovation).

Author contributions

All the authors contributed to the conception and design of the study. Material preparation, data collection, and analyses were performed by MHH, DHL, MSJ, and JWY. The first draft of the manuscript was written by MHH, and all the authors commented on

the previous versions of the manuscript. All authors have read and approved the final manuscript.

Funding

Funding was provided by National Research Foundation of Korea (Grant No.: 2021R1A2C1009714) and Korea Institute for Advancement of Technology (Grant No.: P0008458).

Data availability

We have read and understood your journal's policies and believe that neither the manuscript nor the study violates any of these.

Declarations

Conflict of interest The authors have no relevant financial or non-financial interests to disclose.

References

1. J.W. Yoon, J.W. Kim, J.M. Koo, S.S. Ha, B.I. Noh, W.C. Moon, J.H. Moon, S.B. Jung, *J. Weld. Join.* **25**(2), 6 (2007). <https://doi.org/10.5781/KWJS.2007.25.2.006>
2. J.H. Ahn, K.S. Kim, Y.C. Lee, Y.I. Kim, S.B. Jung, *J. Microelectron. Packag. Soc.* **17**(3), 1 (2010)
3. J.M. Koo, J.W. Kim, J.W. Yoon, B.I. Noh, C.Y. Lee, J.H. Moon, C.D. Yoo, S.B. Jung, *J. Weld. Join.* **26**(1), 31 (2008). <https://doi.org/10.5781/KWJS.2008.26.1.031>
4. J.D. Wu, P.J. Zheng, C.W. Lee, S.C. Hung, J.J. Lee, *Microelectron. Reliab.* **46**(1), 41 (2006). <https://doi.org/10.1016/j.microrel.2005.01.012>
5. S.S. Ha, J.K. Jang, S.O. Ha, J.W. Yoon, H.J. Lee, J.H. Joo, Y.H. Kim, S.B. Jung, *Microelectron. Eng.* **87**(3), 517 (2010). <https://doi.org/10.1016/j.mee.2009.07.015>
6. K.S. Choi, H. Lee, H.C. Bae, Y.S. Oem, *Electron. Telecommun. Trends.* **28**(5), 100 (2013)
7. J.P. Jung, H.Y. Lee, J.H. Cheon, *J. Weld. Join.* **26**(1), 24 (2008). <https://doi.org/10.5781/KWJS.2008.26.1.024>
8. G. Kim, K. Son, G.T. Park, Y.B. Park, *Korean J. Met. Mater.* **55**(11), 798 (2017). <https://doi.org/10.3365/KJMM.2017.55.11.798>
9. J.W. Kim, S.B. Jung, *Int. J. Solids Struct.* **43**(7–8), 1928 (2006). <https://doi.org/10.1016/j.ijsolstr.2005.07.014>
10. J.W. Kim, J.K. Jang, S.O. Ha, S.S. Kim, D.G. Kim, S.B. Jung, *Microelectron. Reliab.* **48**(11–12), 1882 (2008). <https://doi.org/10.1016/j.microrel.2008.07.066>
11. S.Y. Lee, B. Hwang, *Korean. J. Mater. Res.* **26**(5), 281 (2016). <https://doi.org/10.3740/MRSK.2016.26.5.281>
12. J.W. Kim, D.G. Kim, S.B. Jung, *Thin Solid Films* **504**(1–2), 405 (2006). <https://doi.org/10.1016/j.tsf.2005.09.058>
13. I. Shohji, S. Shimoyama, H. Ishikawa, M. Kojima, *J. Jpn. Inst. Electron. Packag.* **1**(1), 9 (2008). <https://doi.org/10.5104/jiepeng.1.9>
14. I. Shohji, T. Yoshida, T. Takahashi, S. Hioki, *Mater. Sci. Eng. A* **366**(1), 50 (2004). <https://doi.org/10.1016/j.msea.2003.09.057>
15. C.K. Hsiung, C.A. Chang, Z.H. Tzeng, C.S. Ho, F.L. Chien, 9th Electronics Packaging Technology Conference, (2007) 719. <https://doi.org/10.1109/EPTC.2007.4469686>
16. A. Mohammadi, R. Mahmudi, *J. Electron. Mater.* **47**(2), 1721 (2018). <https://doi.org/10.1007/s11664-017-5923-9>
17. X. Huang, Z. Wang, Y. Yu, *J. Mater. Res. Technol.* **9**(3), 5533 (2020). <https://doi.org/10.1016/j.jmrt.2020.03.078>

Publisher's Note Springer Nature remains neutral with regard to jurisdictional claims in published maps and institutional affiliations.